Embedded-atom method potential for modeling hydrogen and hydrogen-defect interaction in tungsten

IOP Publishing Journal of Physics: Condensed Matter
J. Phys.: Condens. Matter **29** (2017) 435401 (14pp) https://doi.org/10.1088/1361-648X/aa86bd

Embedded-atom method potential for modeling hydrogen and hydrogen-defect interaction in tungsten

Li-Fang Wang[1,2], Xiaolin Shu[1], Guang-Hong Lu[1] and Fei Gao[2]

[1] Department of Physics, Beihang University, Beijing 100191, People's Republic of China
[2] Department of Nuclear Engineering and Radiological Sciences, University of Michigan, Ann Arbor, MI 48109, United States of America

E-mail: lgh@buaa.edu.cn and gaofeium@umich.edu

Received 7 June 2017, revised 16 August 2017
Accepted for publication 17 August 2017
Published 21 September 2017

Abstract

An embedded-atom method potential has been developed for modeling hydrogen in body-centered-cubic (bcc) tungsten by fitting to an extensive database of density functional theory (DFT) calculations. Comprehensive evaluations of the new potential are conducted by comparing various hydrogen properties with DFT calculations and available experimental data, as well as all the other tungsten–hydrogen potentials. The new potential accurately reproduces the point defect properties of hydrogen, the interaction among hydrogen atoms, the interplay between hydrogen and a monovacancy, and the thermal diffusion of hydrogen in tungsten. The successful validation of the new potential confirms its good reliability and transferability, which enables large-scale atomistic simulations of tungsten–hydrogen system. The new potential is afterward employed to investigate the interplay between hydrogen and other defects, including [1 1 1] self-interstitial atoms (SIAs) and vacancy clusters in tungsten. It is found that both the [1 1 1] SIAs and the vacancy clusters exhibit considerable attraction for hydrogen. Hydrogen solution and diffusion in strained tungsten are also studied using the present potential, which demonstrates that tensile (compressive) stress facilitates (impedes) hydrogen solution, and isotropic tensile (compressive) stress impedes (facilitates) hydrogen diffusion while anisotropic tensile (compressive) stress facilitates (impedes) hydrogen diffusion.

Keywords: interatomic potential, tungsten, hydrogen, defect

(Some figures may appear in colour only in the online journal)

1. Introduction

The critical effects of hydrogen and hydrogen isotopes on the functional properties of tungsten, an appealing plasma-facing material (PFM) used in a thermonuclear fusion device 'tokamak', have been well documented. In the extreme fusion environment, tungsten will be subjected to high hydrogen isotope flux, resulting in sever blistering and cracking on surface [1–5]. The erosion of tungsten caused by hydrogen isotope exposure could introduce tungsten dust into steady-plasma and then lead to detrimental effects on tokamak operation [6, 7]. Meanwhile, the defects and voids caused by neutron irradiation could trap hydrogen isotope and thus increase the retention of hydrogen isotope in tungsten [8–12], which may reduce the utilization of reactant (tritium or deuterium) and increase the safety concern [13]. Recently, Gao *et al* showed the existence of a 10 nm thick deuterium-supersaturated surface layer of tungsten with an unexpectedly high deuterium concentration of similar to 10 at.% after irradiation with ion energy of 215 eV [14], indicating a new pattern of the interplay between deuterium atoms and tungsten lattice. And for studying the dominant physics of trapping and diffusion of deuterium, Barton *et al* proposed a simplified retention model that provides concentration profiles based on experimental

data [15]. Investigating the behavior of hydrogen and its isotopes in tungsten has become one of the most important subjects of the PFM research.

Atomic simulations could provide insights into the microscopic origin and physical mechanisms of the hydrogen effects. However, the ability of atomic simulations to reproduce the behavior and properties of real materials depends on the availability of accurate and computationally efficient interatomic potentials. Unfortunately, the interatomic potentials for a tungsten–hydrogen system are quite rare and defective. In 1975, a potential function describing the interaction of hydrogen molecules with a tungsten [0 0 1] surface was formulated as a modified LEPS potential by McCreery and Wolken [16], which is the first attempt to describe the interaction between hydrogen and tungsten. After that, Juslin *et al* developed an analytical interatomic potential for modeling non-equilibrium processes in a tungsten–carbon–hydrogen system (denoted as Pot_Juslin) [17], and Li *et al* developed a modified analytical interatomic potential for the defective tungsten–hydrogen system (denoted as Pot_Li) [18]. Both Pot_Juslin and Pot_Li are bond-order potentials that are computationally expensive because of the 3-body interaction. Such a shortcoming limits both spatial and temporal scales of simulations, making studying the interplay between hydrogen atoms and extended defects such as dislocations and grain boundaries in tungsten be very difficult. Recently, Bonny *et al* developed an embedded-atom method (EAM) potential (denoted as Pot_Bonny) for large scale atomistic simulations of a ternary tungsten–hydrogen–helium system [19], which shows a higher computational speed than Pot_Li and Pot_Juslin. However, it could not reproduce the formation of hydrogen molecules in vacuum, indicating that the simulations based on Pot_Bonny may not be able to properly model the nucleation of hydrogen molecules and surface blistering in both defective tungsten lattice and vacuum. Thus, available interatomic potentials for a tungsten–hydrogen system are very limited, which obviously impedes the studies of hydrogen effects on tungsten.

In this paper, an efficient and accurate EAM potential (denoted as Pot_present) for a binary tungsten–hydrogen system is developed, and its accuracy and transferability have been thoroughly assessed through the comparison with density functional theory (DFT) calculations, available experimental data and other interatomic potentials. In section 2, we introduce the potential formalism, the fitting methodology and the calculation details. In section 3, performance of the new potential on reproducing and describing properties of a tungsten–hydrogen system is presented and discussed. Finally, conclusions are summarized in section 4.

2. Methods

2.1. Potential formalism

We employ the EAM model for calculating potential energy, which is given by

$$E_{\rm tot} = \sum_i F(\rho_i) + \frac{1}{2}\sum_{i\neq j}\Phi(r_{ij}), \tag{1}$$

where r_{ij} and Φ are the distance and pair potential between atom i and j, respectively, and F is the embedding energy which is a function of atomic electron density ρ and the sums run over all atoms in the system. For tungsten–tungsten interaction, an existing EAM potential with good properties and high reliability, which was developed recently, is adopted where the potential parameters remain unchanged [20]. For tungsten–hydrogen and hydrogen–hydrogen interactions, the analytical potential form used in this work is the same as the model successfully applied to a Ni–H system [21, 22]. In this model, the pair potential between tungsten and hydrogen is given by

$$\begin{aligned}\Phi_{\rm W-H}(r_{ij}) = {} & c_1[{\rm e}^{-2c_2(r_{ij}-c_3)} - 2{\rm e}^{-c_2(r_{ij}-c_3)}]f_{\rm cut}(r_{ij}) \\ & + c_{10\rm W}\rho_{\rm W}(r_{ij}) + c_{10\rm H}\rho_{\rm H}(r_{ij}),\end{aligned} \tag{2}$$

where $f_{\rm cut}(r_{ij})$ is a cut-off function, of which the form is

$$f_{\rm cut}(r_{ij}) = {\rm e}^{\frac{1}{r_{ij}-r_{\rm cut}}}. \tag{3}$$

The electron density of hydrogen is given by

$$\rho(r) = c_4 r^6({\rm e}^{-c_5 r} + 2^9{\rm e}^{-2c_5 r})f_{\rm cut}(r), \tag{4}$$

and the embedding energy for hydrogen is given by

$$F_{\rm H}(\rho) = c_6\rho^2 + c_7\rho + \frac{c_8\rho^{\frac{5}{3}}}{c_9+\rho}. \tag{5}$$

Besides, in order to make the tungsten–hydrogen interaction more adjustable, a relative scaling factor is specified for the density of hydrogen, and the embedding energy of hydrogen also needs to be modified so that the total energy remains unchanged. The invariant transformations are given by

$$\begin{aligned}\rho^*_{\rm H} &= S_{\rm H}\rho_{\rm H}, \\ F^*_{\rm H}(\rho) &= F_{\rm H}(\rho/S_{\rm H}),\end{aligned} \tag{6}$$

where $S_{\rm H}$ is the scaling factor.

In order to reproduce the behavior of hydrogen molecular in vacuum, the pair potential of hydrogen is written as

$$\Phi^*_{\rm H-H}(r_{ij}) = s(r_{ij})\{E_{\rm mol}(r_{ij}) - 2F^*_{\rm H}[\rho^*_{\rm H}(r_{ij})]\} + [1-s(r_{ij})]\Phi_{\rm H-H}, \tag{7}$$

$$\begin{aligned}\Phi_{\rm H-H}(r_{ij}) = {} & c_{\rm H1}[{\rm e}^{-2c_{\rm H2}(r_{ij}-c_{\rm H3})} - 2{\rm e}^{-c_{\rm H2}(r_{ij}-c_{\rm H3})}]f_{\rm cut}(r_{ij}) \\ & + c_{\rm H10H}\rho_{\rm W}(r_{ij}) + c_{\rm H10H}\rho_{\rm H}(r_{ij}),\end{aligned} \tag{8}$$

$$s(r_{ij}) = 0.5\{1 - \tanh[15(r_{ij}-0.9)]\}, \tag{9}$$

$$E_{\rm mol}(r_{ij}) = -4.74(1+a^\dagger){\rm e}^{-a^\dagger}, \tag{10}$$

$$a^\dagger = (r_{ij}-r_0)/(r_0\lambda), \tag{11}$$

where r_0 is the equilibrium separation of 0.74 Å for hydrogen molecules, and $\lambda = 0.4899$. $s(r_{ij})$ switches the hydrogen pair interaction rapidly from the EAM model to the Rose equation of state [23] at a distance of 0.9 Å. However, it should be noted that within this model, even in the tungsten matrix, hydrogen tends to be trapped in the deep hydrogen molecule potential well once the distances among them are below 0.9 Å, which is inconsistent with the DFT predictions. Hence, in

order to balance the strong pair potential resulting from the Rose equation [23], the embedding energy is increased by modifying the electronic density function of hydrogen ρ_{H} as

$$\rho_{\mathrm{H}} = \begin{cases} \rho(r_c), & r \leqslant r_c \\ \rho(r), & r > r_c \end{cases}, \tag{12}$$

where $\rho(r)$ is the density function defined by equation (4), r_c is the extremum of $\rho(r)$ and $r_c = 0.568\ 0335$ Å. Such modifications remain other properties of the potentials unchanged.

In the potential formulism above, c_1, c_2, c_3, $c_{10\mathrm{W}}$, $c_{10\mathrm{H}}$, c_4, c_5, c_6, c_7, c_8, c_9, c_{H1}, c_{H2}, c_{H3}, c_{H10W}, c_{H10H}, r_{cut}, S_{H}, c_1, c_1 are all fitting parameters, which are adjusted to give desired properties of a tungsten–hydrogen system.

2.2. Fitting methodology

The new potential is fitted based on DFT calculations, and the database includes the formation energy of a substitutional and an interstitial hydrogen atom in body-centered-cubic (bcc) tungsten, the binding energy of two hydrogen atoms in different configurations in bulk tungsten, the energy and sites of hydrogen atoms binding to a monovacancy in tungsten, and the formation energy of some important molecules, such as H_2, WH and so on. Due to the lightness of hydrogen atoms, some properties in the fitting database will be considerably affected by zero-point energy (ZPE) correcting, such as the formation energy of hydrogen atom at substitutional or interstitial sites, the binding energy of a hydrogen atom to a monovacancy, and so on. The values of these properties after ZPE correcting will be about 0.2 eV higher, as shown in table 3. Therefore, for these properties, we put the 'ZPE-corrected' energies in the fitting database and the present W–H potential could be employed to modeling the systems which do not need further ZPE corrections. The whole database is listed in table 1.

For the fitting procedure, the least square method is employed and the objective function U is defined as

$$U = \sum_i w_i [f_i(\lambda^n) - F_i]^2, \tag{13}$$

where f_i is the calculated property, λ^n is the potential parameter set, F_i is the reference value to be fitted as shown in the database, and w_i is the weight of each property item i in the fitting process. As described by Gao *et al* [24], the atomic configurations of hydrogen defects and clusters are spontaneously relaxed using a conjugate gradient algorithm implemented in the molecular dynamics code LAMMPS [25] to obtain the fitting properties f_i, and the size of simulation supercell is $10 \times 10 \times 10\ a_0^3$, where a_0 is the lattice constant of bcc tungsten. Based on equation (13), the potential parameter set λ^n is adjusted repeatedly until the objective function U is minimized. Parameters of the new potentials resulting from above fitting procedure are given in table 2.

2.3. Calculation details

2.3.1. MD/MS calculations. Molecular dynamics (MD) and molecular statics (MS) simulations were performed using LAMMPS codes [25]. Unless otherwise specified, the size of simulation supercell is $10 \times 10 \times 10\ a_0^3$ where a_0 is the lattice constant of bcc tungsten, containing 2000 tungsten atoms, desired defects and hydrogen atoms. Larger simulation cells were tested to ensure such size of simulation supercell is large enough for calculating defect properties. In all the simulations, periodic boundaries were applied.

The formation energy of a defect is calculated as

$$E_{\mathrm{f}} = E_{\mathrm{def}} - [E_{\mathrm{ref,W}} \cdot (N - m_{\mathrm{vac}})/N + E_{\mathrm{ref,H}} \cdot n_{\mathrm{H}}], \tag{14}$$

where E_{def} is the energy of the system with desired defects, $E_{\mathrm{ref,W}}$ is the reference energy of the pure tungsten matrix, N is the number of tungsten atoms in the reference matrix and m_{vac} is the number of vacancies in the final defective system. The reference energy used for hydrogen, $E_{\mathrm{ref,H}}$, is the half of

Table 1. Database for fitting the new potential. $E^{\mathrm{H}}_{\mathrm{f,ss}}$, $E^{\mathrm{H}}_{\mathrm{f,tet}}$ and $E^{\mathrm{H}}_{\mathrm{f,oct}}$ are the formation energy of a hydrogen atom at substitutional, tetrahedral interstitial, and octahedral interstitial sites (denoted as OIS) in bcc tungsten, respectively. $\Delta E^{\mathrm{H}}_{\mathrm{f,oct-tet}}$ is the difference of $E^{\mathrm{H}}_{\mathrm{f,tet}}$ and $E^{\mathrm{H}}_{\mathrm{f,oct}}$. $E^{\mathrm{H}\to\mathrm{V}}_{\mathrm{B}}$ and $E^{\mathrm{H}\to\mathrm{H_1V_1}}_{\mathrm{b}}$ are the binding energy of a hydrogen atom to a monovacancy (denoted as V) and a hydrogen-vacancy cluster (denoted as $\mathrm{H}_n\mathrm{V}_m$, where n is the number of hydrogen atoms and m is the number of vacancies in the cluster), respectively. $P^{\mathrm{H_1V_1}}$, $P_1^{\mathrm{H_2V_1}}$ and $P_2^{\mathrm{H_2V_1}}$ are the positions of a hydrogen atom in a monovacancy, the first and second hydrogen atom in a $\mathrm{H_2V_1}$ cluster, respectively, and a_0 is the lattice constant of bcc tungsten. $E_{\mathrm{f}}^{\mathrm{H_2}}$, $E_{\mathrm{f}}^{\mathrm{WH_1}}$ and $E_{\mathrm{f}}^{\mathrm{WH_4}}$ are the formation energy of hydrogen and tungsten–hydrogen molecules in vacuum, and $D^{\mathrm{H_2}}$ is the bond length of a hydrogen molecule in vacuum. $E_{\mathrm{b}}^{\mathrm{2H_A}}$, $E_{\mathrm{b}}^{\mathrm{2H_B}}$, $E_{\mathrm{b}}^{\mathrm{2H_C}}$, $E_{\mathrm{b}}^{\mathrm{2H_D}}$, $E_{\mathrm{b}}^{\mathrm{2H_E}}$, $E_{\mathrm{b}}^{\mathrm{2H_F}}$ and $E_{\mathrm{b}}^{\mathrm{2H_G}}$ are the binding energy of two hydrogen atoms at different TISs, where the subscript A to G indicates difference configurations as shown in figure 1.

Properties	Reference value
$E^{\mathrm{H}}_{\mathrm{f,ss}}$ (eV)	4.25[a]
$E^{\mathrm{H}}_{\mathrm{f,tet}}$ (eV)	1.00[a]
$E^{\mathrm{H}}_{\mathrm{f,oct}}$ (eV)	1.38[a]
$\Delta E^{\mathrm{H}}_{\mathrm{f,oct-tet}}$ (eV)	0.38[a]
$E_{\mathrm{b}}^{\mathrm{H}\to\mathrm{V}}$ (eV)	1.41[a]
$P^{\mathrm{H_1V_1}}$ (Å)	0.10 a_0 off OIS[a]
$E_{\mathrm{b}}^{\mathrm{H}\to\mathrm{H_1V_1}}$ (eV)	1.40[a]
$P_1^{\mathrm{H_2V_1}}$ (Å)	0.10 a_0 off OIS[a]
$P_2^{\mathrm{H_2V_1}}$ (Å)	0.90 a_0 off OIS[a]
$E_{\mathrm{f}}^{\mathrm{H_2}}$ (eV)	−4.74
$D^{\mathrm{H_2}}$ (Å)	0.74
$E_{\mathrm{f}}^{\mathrm{WH_1}}$ (eV)	−2.95
$E_{\mathrm{f}}^{\mathrm{WH_4}}$ (eV)	−9.69
$E_{\mathrm{b}}^{\mathrm{2H_A}}$ (eV)	−0.47
$E_{\mathrm{b}}^{\mathrm{2H_B}}$ (eV)	−0.11
$E_{\mathrm{b}}^{\mathrm{2H_C}}$ (eV)	−0.04
$E_{\mathrm{b}}^{\mathrm{2H_D}}$ (eV)	0.01
$E_{\mathrm{b}}^{\mathrm{2H_E}}$ (eV)	0.000
$E_{\mathrm{b}}^{\mathrm{2H_F}}$ (eV)	−0.03
$E_{\mathrm{b}}^{\mathrm{2H_G}}$ (eV)	−0.05

[a] The reference values is derived with ZPE correction.

Table 2. Parameters for the new potentials. Energy and distances are in eV and Å, respectively.

Parameters	Values
c_1	0.057 773 582 534
c_2	2.366 659 792 062
c_3	2.539 095 864 581
c_{10W}	0.0
c_{10H}	0.0
c_4	74.726 706 479 776
c_5	5.311 164 848 925
c_6	4.366 867 287 278
c_7	−28.445 955 150 459
c_8	27.753 023 506 211
c_9	0.221 071 572 489
c_{H1}	−0.022 694 666 425
c_{H2}	30.593 831 601 003
c_{H3}	0.003 294 745 046
c_{H10W}	0.0
c_{H10H}	0.0
r_{cut}	3.2 (ρ)
	3.2 (Φ_{H-H})
	4.7 (Φ_{W-H})
S_H	4.748 409 674 167

the energy of a hydrogen molecule in vacuum, and n_H is the number of hydrogen atoms in the final defective system.

The binding energy of hydrogen atoms to a defect (denoted as X), $E_b(H \to X)$, is defined as

$$E_b(H \to X) = [E_{TIS}(H) + E(X)] - [E(HX) + E_{ref,W}], \quad (15)$$

where $E_{TIS}(H)$ is the energy of a system with a single hydrogen atom at the tetrahedral interstitial site (TIS), $E(X)$ is the energy of the system with the defect, $E(HX)$ is the energy of a system with the HX cluster, and $E_{ref,W}$ is the reference energy of the pure tungsten matrix. X could be a hydrogen atom, self-interstitial atom (SIA), a vacancy or a vacancy cluster. By such definition, the positive binding energy indicates an energetically attraction between hydrogen atoms and defects. In the case of a hydrogen atom binding to another hydrogen atom in tungsten,

$$E_b(H \to H) = 2E_{TIS}(H) - [E(H_2) + E_{ref,W}], \quad (16)$$

where $E(H_2)$ is the energy of the system with two hydrogen atoms. In the case of a sequential hydrogen atom binding to a [1 1 1] SIA,

$$E_{b,s}(H \to H_{n-1}SIA) = [E_{TIS}(H) + E(H_{n-1}SIA)] - [E(H_nSIA) + E_{ref,W}], \quad (17)$$

where n is the number of hydrogen atoms bound to the SIA. In the case of a sequential hydrogen atom binding to a vacancy or a vacancy cluster,

$$E_{b,s}(H \to H_{n-1}V_m) = [E_{TIS}(H) + E(H_{n-1}V_m)] - [E(H_nV_m) + E_{ref,W}], \quad (18)$$

where V denotes vacancy and m is the number of vacancies. In the case of total binding energy of n hydrogen atoms bound to a vacancy or a vacancy cluster,

$$E_{b,t}(H_n \to V_m) = [n \cdot E_{TIS}(H) + E(V_m)] - [E(H_nV_m) + n \cdot E_{ref,W}]. \quad (19)$$

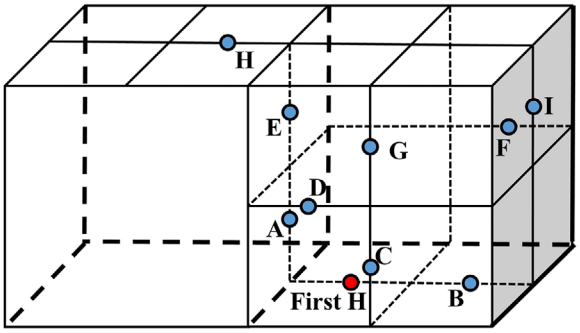

Figure 1. Configurations of two hydrogen atoms at TISs of bcc tungsten. The red sphere indicates the first hydrogen atom, and the blue spheres indicates the second hydrogen atoms.

In order to obtain the binding energy and structure of a defect cluster, we apply the MS minimization to the system at 0 K. For calculating the binding energy of multiple hydrogen atoms in bulk tungsten, hydrogen atoms are separately placed at different TISs which are the most stable interstitial sites for them in tungsten, as shown in figure 1, and then the whole system is energetically minimized at 0 K. In the case of a hydrogen-SIA cluster, we first create a [1 1 1] SIA, which is the most stable SIA structure in tungsten, and then add 1 to 12 hydrogen atoms randomly around the [1 1 1] SIA, after which the energetic minimization is applied to the whole system. Such procedure is repeated for 100 000 times for each cluster, and then the result with the lowest energy, which indicates the most stable structure, is selected as the ground state of the cluster. Since it is hard to ensure the actual ground state of a cluster, there is a possibility that the results we selected are metastable states. However, the massive repetitions guarantee the selected results will be very close to, if not equal to, the ground states. Similar calculations and selection processes are also applied to the hydrogen-vacancy clusters. We firstly create a monovacany or a vacancy cluster with m vacancies, which is achieved by relaxing an $m-1$ cluster at 0 K and then removing the tungsten atom with the highest potential energy. After that, 1 to $10 \times m$ hydrogen atoms are added in the monovacancy or vacancy cluster, then energetic minimization is applied to the whole system. Such procedure is repeated for 2000 times for each cluster, after which the results with the lowest energy are selected as the ground states of the clusters.

The solution energy of hydrogen in strained tungsten is calculated as

$$E_{s,\varepsilon} = E_{H,\varepsilon} - (E_{ref,W_\varepsilon} + E_{ref,H}), \quad (20)$$

where ε is the strain applied to the supercell, $E_{H,\varepsilon}$ is the energy of a strained system with a hydrogen atom at TIS, E_{ref,W_ε} is the reference energy of the pure strained tungsten matrix, and $E_{ref,H}$ is the half of the energy of a hydrogen molecule in vacuum. A nudged elastic band [26, 27] calculation is performed to calculate the diffusion energy barrier of a hydrogen atom for the hop path between the nearest TISs, as shown in figure 9, in a strained tungsten.

In order to simulate the thermal diffusion of hydrogen in tungsten, MD simulation is carried out. The simulation box is $12 \times 12 \times 12\ a_0^3$, where a_0 is the lattice constant of bcc

Table 3. Point defect properties of hydrogen in tungsten. $E^{H}_{f,ss}$, $E^{H}_{f,tet}$ and $E^{H}_{f,oct}$ are the formation energy of a hydrogen atom at substitutional, tetrahedral interstitial, and octahedral interstitial sites in bcc tungsten, respectively. $E^{H}_{m,t\to t}$ is the migration energy of a hydrogen atom between two nearest neighbor TISs in bcc tungsten. $E^{H_2}_{f}$ is the formation energy of a hydrogen molecule in vacuum. For DFT calculations, both the results with ZPE and without ZPE are included.

	DFT							
Properties	Without ZPE	With ZPE	Experiment	Pot_present	Pot_Bonny1	Pot_Bonny2	Pot_Li	Pot_Juslin
$E^{H}_{f,ss}$ (eV)	4.08[a], 4.24[b]			3.988	5.89	−17.65	4.04	4.06
$E^{H}_{f,tet}$ (eV)	0.88[a], 0.86[b], 0.85[c], 0.87[d]	1.00[e], 1.09[d]	1.04 ± 0.17[f]	1.05	3.65	−19.86	0.86	1.04
$E^{H}_{f,oct}$ (eV)	1.26[a], 1.26[b], 1.33[c]	1.38[e]		1.40	3.99	−19.48	1.18	1.40
$E^{H}_{m,t\to t}$ (eV)	0.20[a], 0.21[c], 0.42[b]	0.38[b]	0.39[f]	0.22	0.22[g]	0.21[g]	0.23	0.34 ± 0.03[h]
$E^{H_2}_{f}$ (eV)				−4.72			−4.75	−4.75

[a] Reference [39].
[b] Reference [72].
[c] Reference [67].
[d] Reference [47].
[e] Reference [61].
[f] Reference [65].
[g] Reference [19].
[h] Reference [17].

tungsten, containing 3456 tungsten atoms and 1 hydrogen atom, i.e. the concentration of hydrogen in tungsten is about 0.03 at.%. The Nose–Hoover style thermostat/barostat [28] are employed to maintain the temperature of the system at a desired value and the pressure of the system at 0 kbar. The equations of motion used were those of Shinoda *et al* [29], which combine the hydrostatic equations of Martyna *et al* [30] with the strain energy proposed by Parrinello and Rahman [31]. The time integration schemes closely follow the time-reversible measure-preserving Verlet integrators derived by Tuckerman *et al* [32]. The diffusion simulation is run for 500 ps with a time step of 0.0001 ps.

2.3.2. DFT calculations. DFT calculations were performed using the pseudopotential plane-wave method as implemented in the VASP code [33, 34]. The generalized gradient approximation of Perdew and Wang [35] and projected augmented wave potentials [36] are employed with a plane-wave energy cutoff of 350 eV. The size of the supercell is $4 \times 4 \times 4$ a_0^3, where a_0 is the lattice constant of bcc tungsten containing 128 tungsten atoms and desired defects, and the Brillouin zone is sampled with $3 \times 3 \times 3$ k points by the Monkhorst–Pack scheme [37]. The energy minimization is continued until the forces on all the atoms are converged to less than 10^{-3} eV Å^{-1}. Besides, for calculating the solution energy of hydrogen in a strained tungsten, the ZPE of hydrogen is taken into account by summing up the zero-point vibrational energy of hydrogen normal modes.

3. Results and discussion

In this section, a comprehensive assessment of the new tungsten–hydrogen potential is provided. Firstly, we examine the point defects properties of hydrogen in tungsten. Then interaction between hydrogen and various defects in tungsten are investigated. Specifically, we carry out a detailed study on how hydrogen atoms bind to the other hydrogen atoms, SIAs, a monovacancy and vacancy clusters in tungsten. Next, we calculate the solution and diffusion of hydrogen in strained bulk tungsten, paying attention to the effects of both isotropic and anisotropic strain. Finally, the thermal diffusion of hydrogen in tungsten is examined, as a test case for the thermal properties of the new potential.

3.1. Point defect properties of hydrogen

Point defect properties of hydrogen in tungsten, including the formation energy of a hydrogen atom at substitutional and interstitial sites and the migration energy of a hydrogen atom between two nearest TISs, are calculated based on Pot_present. For comparison, DFT calculations, available experimental data and results from other interatomic potentials (Pot_Bonny1, Pot_Bonny2, Pot_Li, and Pot_Juslin) are also derived. Results are shown in table 3. Compared with DFT calculations with ZPE, Pot_present accurately reproduces the formation energy of a hydrogen atom at substitutional, tetrahedral and octahedral interstitial sites (OISs), respectively. The migration energy of a hydrogen atom between two nearest neighbor TISs calculated by Pot_present is in good agreement with DFT calculation without ZPE, though it is lower than experimental data. Such agreement indicates good transferability of Pot_present since the migration energy of a hydrogen atom in tungsten is not included in the fitting database. Other potentials also show good performances on these energetic calculations, as indicated in table 3. In particular, even though the results from Pot_Bonny1 and Pot_Bonny2 do not match the DFT calculations quantitatively, they correctly reproduce the relative stability of different hydrogen atom interstitial occupation sites in tungsten, which makes them still convincing in simulating hydrogen behaviors in tungsten qualitatively.

Besides, as shown in table 3, the formation of hydrogen molecules in vacuum is also confirmed, which verifies the reliability of Pot_present in modeling the nucleation of hydrogen bubble and the blistering process on tungsten surface.

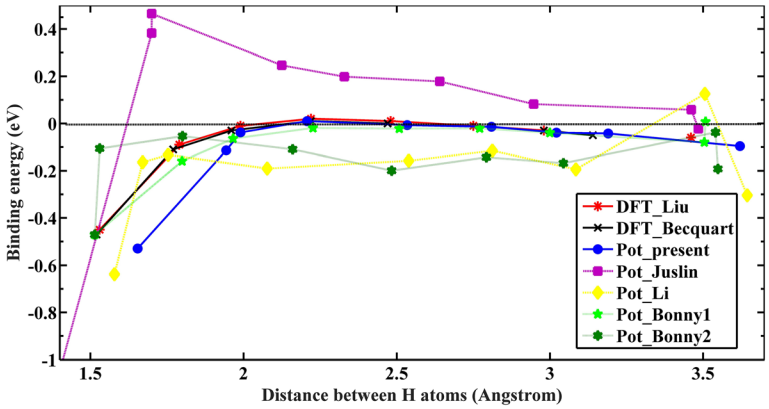

Figure 2. Binding energy of two hydrogen atoms at TISs, given by equation (16) of the text, as a function of their distance in tungsten.

3.2. Interactions between hydrogen and defects

In bcc tungsten matrix, defects could play a dominate role in affecting the behavior of hydrogen [38]. Understanding how hydrogen interacts with various defects in tungsten is crucial for further studies of tungsten–hydrogen system. In this part, we mainly consider three kinds defects to which hydrogen may bind in tungsten, including hydrogen atom themselves, SIAs, and vacancy clusters. How hydrogen interacts with these defects is studied in detail using Pot_present and other interatomic potentials, with the available DFT calculations presented for comparison.

3.2.1. Interaction between hydrogen atoms in perfect tungsten. In order to explore the probability of hydrogen forming hydrogen molecules in intrinsic tungsten, the interaction between hydrogen atoms in perfect tungsten has been extensively studied by DFT calculations [39–42]. It is confirmed that the interaction between two hydrogen atoms in tungsten is nearly repulsive, and only at a distance of 2.2 Å will the two hydrogen atoms show a very low binding energy which is less than 0.1 eV. This may suggest that hydrogen atoms are hardly clustering and forming hydrogen molecules in a perfect tungsten matrix, as confirmed by the kinetic Monte Carlo (KMC) simulations [40]. Undoubtedly, a good tungsten–hydrogen potential should be able to reproduce above results, which makes it convincing to describe the interaction among hydrogen atoms in tungsten. Hence, the binding energy of hydrogen atoms in a perfect bulk tungsten is calculated using Pot_present and other interatomic potentials, and the results are shown in figure 2 and table 4. Available DFT data derived from two different groups [39, 42] (denoted as DFT_Liu and DFT_Becquart) are also presented in figure 2 and table 4 for comparison.

As shown in figure 2, the results obtained with Pot_present are in an excellent agreement with the DFT calculations. Pot_present successfully reproduces the weak binding between two hydrogen atoms at the distance of 2.2 Å, even though it slightly overestimates the repulsive interaction between hydrogen atoms at a short distance. The binding energy given by Pot_Juslin shows much stronger attractive interaction between hydrogen atoms, resulting in an energetics preference for hydrogen to form clusters in a perfect bulk tungsten, which is contrary to the DFT predictions. In contrast, both Pot_Li and Pot_Bonny2 predict repulsive interactions between two hydrogen atoms at all the configurations, failing in reproducing the weak binding at 2.2 Å as predicted by DFT calculations. Pot_Bonny1 predicts more reasonable results though it slightly underestimates the binding energy compared with the DFT calculations. Overall, Pot_present and Pot_Bonny1 show better performance on describing the interaction between hydrogen atoms in a perfect bulk tungsten.

Table 4. Binding energy and bond lengths of two hydrogen atoms at different TISs of bcc tungsten, as shown in figure 1.

	Pot_present		DFT_ Becquart[a]		DFT_Liu[b]	
Configuration	*E* (eV)	*D* (Å)	*E* (eV)	*D* (Å)	*E* (eV)	*D* (Å)
A	−0.47	1.72	−0.47	1.52	−0.45	1.53
B	−0.11	1.98	−0.11	1.77	−0.09	1.79
C	−0.04	2.03	−0.03	1.96	−0.01	1.99
D	0.01	2.23	0.01	2.22	0.02	2.22
E	0.01	2.50	0	2.47	0.01	2.48
F	0.00	2.75			−0.01	2.75
G	−0.03	2.98	−0.03	2.98	−0.03	2.98
H	0.01	3.50	−0.11	1.77		
I	−0.07	3.52			−0.06	3.46

[a] Reference [42].
[b] Reference [39].

3.2.2. Interaction between hydrogen and [1 1 1] SIAs. SIAs along the [1 1 1] direction are the most stable interstitial structure in tungsten, and often have significant effects on the evolution of extended defects, such as dislocations and grain boundaries. Also, since the remarkable diffusivity difference between a [1 1 1] SIA and a vacancy may impede the self-healing process of Frenkel defects in tungsten, hydrogen may be able to offer trap sites to lower the mobility of the [1 1 1] SIA, increasing the recombination probability of the Frenkel defects. Therefore, quantifying the interaction between hydrogen and a [1 1 1] SIA is quite necessary. Heinola *et al* calculated that the binding energy of a hydrogen atom to a [1 1 1] SIA of tungsten is 0.43 eV [43], which is the only *ab initio* data we could refer to for now. Recently, Kato *et al* revealed

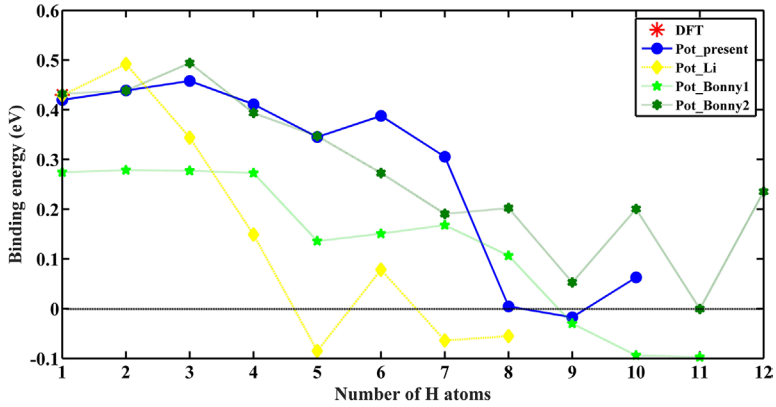

Figure 3. Binding energy of a sequential hydrogen atom to a $H_{n-1}SIA$ cluster, given by equation (17) of the text, as a function of hydrogen atom number (n).

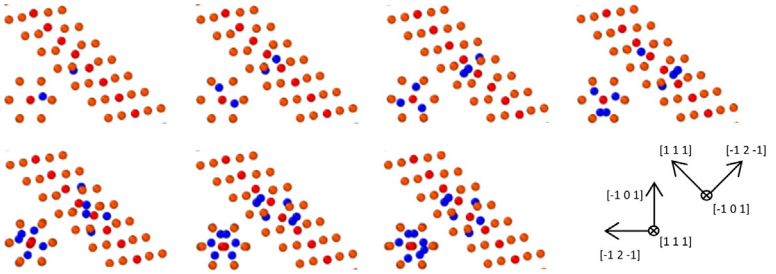

Figure 4. Binding configurations of hydrogen atoms to a [1 1 1] SIA of bcc tungsten. Blue spheres are hydrogen atoms, and red and orange spheres are tungsten atoms.

that hydrogen clusters can prevent a vacancy from recombining with the neighboring crowdion-type SIA by DFT molecular dynamics [44], but how hydrogen affect the motion of a [1 1 1] SIA has not been investigated. Therefore, to understand the interplay between hydrogen and a [1 1 1] SIA in tungsten, we calculate the binding energy of hydrogen atoms to a [1 1 1] SIA, and for comparison, the results from other potentials are also derived.

As shown in figure 3, obviously, all the interatomic potentials show the binding energy of hydrogen atoms to a [1 1 1] SIA will decrease with the number of hydrogen atoms. This indicates that the ability of a [1 1 1] SIA for trapping hydrogen will be weaken by the presence of the surrounding hydrogen atoms, which indirectly confirms that there is a basically repulsive interaction between hydrogen atoms in tungsten. In addition to the overall decreasing trend, however, it should be noted that the binding energy predicted by Pot_present shows a slight increase when the numbers of hydrogen atoms are three and six. We believe that this may be caused by the symmetry of the arrangement of hydrogen atoms around the [1 1 1] SIA, which lowers the formation energy of the defect clusters and results in the increase of the binding energy. Further checking of hydrogen atom configurations around the [1 1 1] SIA confirms our hypothesis, as shown in figure 4. When there are three hydrogen atoms around the [1 1 1] SIA, the arrangement of hydrogen atoms shows a three-fold rotational symmetry with respect to the [1 1 1] direction, thus resulting in the highest binding energy; when there are six hydrogen atoms around the [1 1 1] SIA, the arrangement of hydrogen atoms shows a central symmetry with respect to the center of [1 1 1] crowdion, resulting in a relative higher binding energy. The considerable positive binding energy between hydrogen and the [1 1 1] SIA also indicate that hydrogen indeed has trapping effects on the [1 1 1] SIA in tungsten and may lower the mobility of the [1 1 1] SIA, which mitigates the difference of mobility between SIAs and vacancies and could result in increasing the recombination probability of Frenkel pairs. Finally, according to figure 3, a [1 1 1] SIA may be able to trap at most 7, 4, 8, 10 hydrogen atoms, as calculated by Pot_present, Pot_Li, Pot_Bonny1, and Pot_Bonny2, respectively.

3.2.3. Interaction between hydrogen and vacancies. Vacancies and vacancy-type defects are believed to be main trapping sites for hydrogen in tungsten. Since the effects of the interplay between hydrogen and vacancies on the mechanical properties of tungsten are still unclear, many researches on this theme have been conducted based on DFT calculations and thermodynamics theories [42, 43, 45–55]. DFT calculations confirm that there is a strong attractive interaction between hydrogen and vacancies. The binding energy of a single hydrogen atom to a monovacancy, with zero-point vibrations taken into account, is 1.26 eV by Fernandez *et al* [45], 1.43 eV by Heinola *et al* [43], 1.36 eV by You *et al* [56], and 1.318 eV by Ohsawa *et al* [54], and a monovacancy is predicted to be able to accommodate up to about 12 hydrogen atoms at 0 K. Kato *et al* calculated the binding energy of a single hydrogen atom to a first-nearest-neighbor and a second-nearest-neighbor di-vacancy are 1.80 eV and 2.15 eV, respectively [52], indicating a di-vacancy has stronger attractions to hydrogen than a monovacancy. Due to the scale limitation of

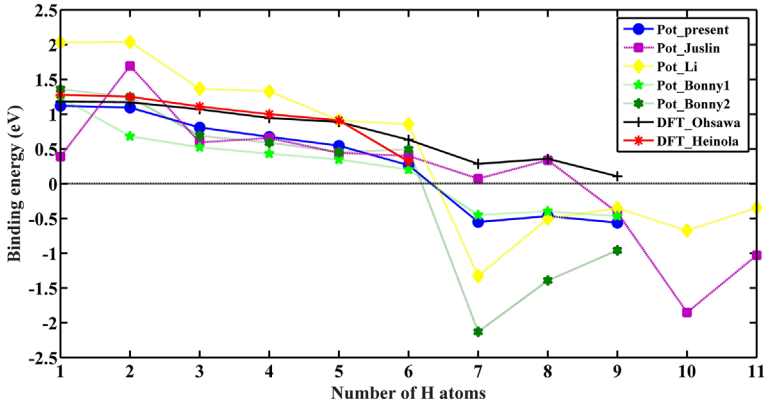

Figure 5. Binding energy of a sequential hydrogen atom to a hydrogen-monovacancy cluster ($H_{n-1}V_1$), given by equation (18) of the text, as a function of hydrogen atom number (n) in tungsten.

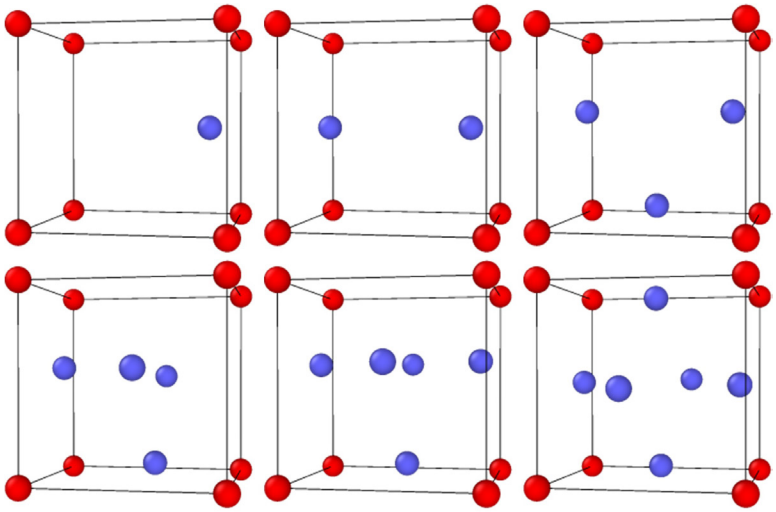

Figure 6. Binding configurations of hydrogen atoms in a monovacancy in tungsten. Blue spheres are hydrogen atoms, and red spheres are tungsten atoms.

DFT calculations, the calculations of binding energy between hydrogen and larger vacancy clusters are too computationally expensive, even though they are crucial to understand the interplay between hydrogen and vacancies for resolving the surface blistering issue in tungsten. The development of a new accurate interatomic potential, which offers a much more efficient calculation yet still retains the details of modeling individual atoms, makes such investigations possible. Hence, here, we calculate the binding energy of hydrogen atoms to a monovacancy, compared with available DFT calculations [43, 54] (denoted as DFT_Ohsawa and DFT_Heinola), as a test of performance for Pot_present. Then, the interaction between hydrogen and vacancy clusters is investigated by Pot_present, as well as other potentials.

Figure 5 shows the binding energy of a sequential hydrogen atom to a monovacnacy-hydrogen cluster in tungsten. All the potentials show that the binding energy decreases with the number of hydrogen atoms in the monovacancy, which is consistent with the DFT calculations. In particular, the binding energy predicted by the Pot_present is slightly lower than that from DFT calculations, especially when the monovacancy contains more than six hydrogen atoms. Also, the maximum number of hydrogen atoms that can be accommodated in a monovacancy calculated by the Pot_present is six, which is less than that calculated by the DFT. However, the sites occupied by hydrogen atoms in a monovacancy, as shown in figure 6, are exactly the same as those predicted by the DFT calculations [54], which is believed to be a considerable advantage of Pot_present to simulate the interplay between hydrogen and vacancies in tungsten. As for other potentials, both Pot_Bonny1 and Pot_Bonny2 underestimate the binding energy between hydrogen and a monovacancy, while Pot_Li overestimates it. The binding energy predicted by Pot_Juslin has an unreasonable increase when there are two hydrogen atoms in the monovacancy, i.e. a hydrogen atom binding to a H_1V_1 cluster. After checking the atomic configuration of this binding cluster, we found that the reason causing such unreasonable results is that the cutoff of the tungsten-hydrogen interaction (2.15 Å) given by Pot_Juslin is so small that the hydrogen atoms siting at the center of the monovacancy will not be affected by the nearest tungsten atoms (2.74 Å), and will be easy to bind to each other, forming hydrogen molecules. Such result clearly contradicts the DFT calculations, and may make Pot_Juslin improperly simulate hydrogen-vacancy interaction. Overall, the Pot_present gives a reasonable performance on describing the interaction between hydrogen and a monovacancy in tungsten.

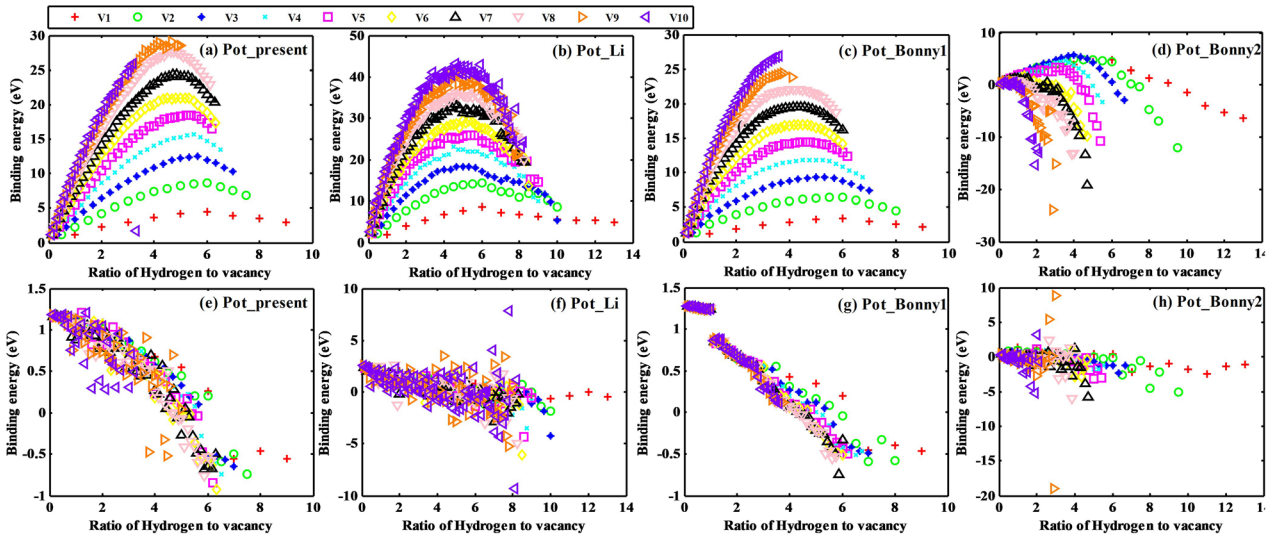

Figure 7. Binding energy of hydrogen atoms to a hydrogen-vacancy cluster in tungsten as a function of the ratio of hydrogen atoms to vacancies. Figures (a)–(d) are the total binding energy, given by equation (19) of the text, calculated by Pot_present, Pot_Li, Pot_Bonny1 and Pot_Bonny2, respectively. Figures (e)–(h) are the sequential binding energy, given by equation (18) of the text, calculated by Pot_present, Pot_Li, Pot_Bonny1 and Pot_Bonny2, respectively. V1, V2, V3, V4, V5, V6, V7, V8, V9 and V10 are vacancy clusters containing 1, 2, 3, 4, 5, 6, 7, 8, 9 and 10 vacancies, respectively. The ratio of hydrogen atoms to vacancies equal n/m, where n is the number of hydrogen atoms and m is the number of vacancies.

Given its good performance on describing interaction between hydrogen and monovacancy in tungsten, the Pot_present is employed to study the interaction between hydrogen and vacancy clusters in tungsten. The total and sequential binding energy of hydrogen atoms to vacancy clusters is calculated using Pot_Present as well as other potentials including Pot_Li, Pot_Bonny1, and Pot_Bonny2. Pot_Juslin is not considered because of its unreasonable performance on calculating the interaction between hydrogen and vacancies. Results are displayed as a function of the ratio of hydrogen atoms (the number of which is denoted as n) to vacancies (the number of which is denoted as m), as shown in figure 7.

In figures 7(a)–(c), the maximum hydrogen inventory of a vacancy cluster, based on Pot_present, Pot_Li and Pot_Bonny1, increases as the size of vacancy clusters grows, suggesting that in a vacancy-assisted hydrogen bubble formation process [38, 46, 48, 57], the vacancy cluster must be large enough to allow more hydrogen atoms to gather and cluster. Besides, the highest total binding energy seems to be at a fixed value of n/m, which is approximately at the range from 5 to 6, regardless the size of vacancy clusters, indicating that the most stable vacancy-hydrogen cluster in tungsten should be V_mH_{5m}. However, Pot_Bonny2 exhibits a different pattern on the total binding energy, as seen in figure 7(d). The total hydrogen inventory of a vacancy cluster derived from Pot_Bonny2 does not depend on the cluster size. In fact, the maximum hydrogen atom number in the clusters predicted by Pot_Bonny2 seems to be a constant, which is at the range of 6–10, regardless to the increase of the vacancy cluster size. Such a performance of Pot_Bonny2 is considered unphysical, since it restricts the possibility of forming large hydrogen clusters and hydrogen bubbles, which is against to the experiment observations [58–60].

In figures 7(e)–(h), all the potentials show a decreasing sequential binding energy of a hydrogen atom to a vacancy cluster, indicating that it would be harder for additional

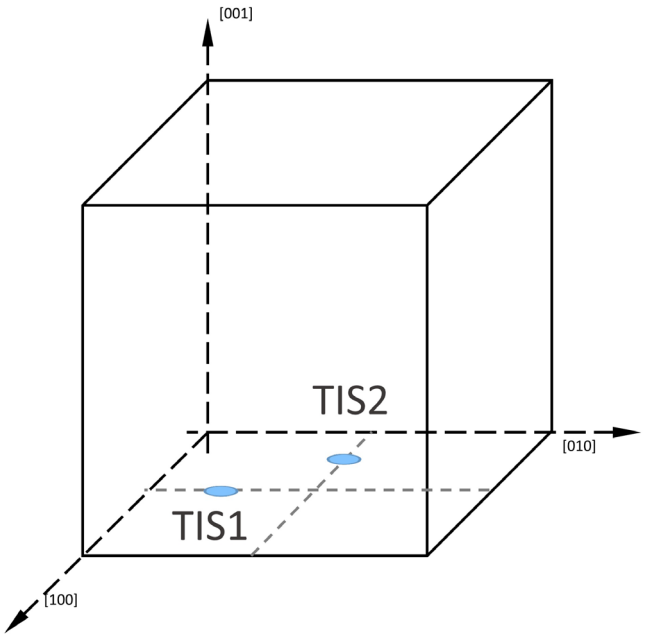

Figure 8. Schematic showing two TISs in a bcc tungsten lattice.

hydrogen atoms to bind to the vacancy clusters as the hydrogen inventory increases. The sequential binding energy of a hydrogen atom predicted by Pot_present seems constant when the ratio of hydrogen to vacancy is less than 1, meaning that when there are more vacancies than hydrogen atoms, the ability of a vacancy cluster for trapping hydrogen will not be affected by changing the cluster size. This is considered reasonable since hydrogen atoms prefer to occupy the edges of vacancies, i.e. the OISs, instead of the centers of vacancies, which has been confirmed by DFT calculations [43, 48, 54]. However, none of other potentials exhibits this detailed information. Pot_Li shows a nearly linear decrease in sequential hydrogen binding energy as the ratio increases. The sequential

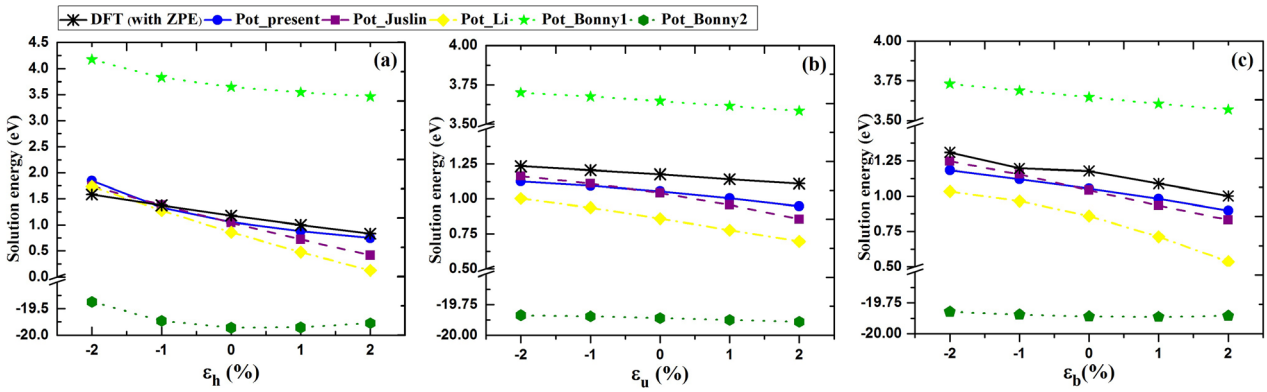

Figure 9. Solution energy of hydrogen in tungsten as a function of (a) hydrostatic, (b) uniaxial, and (c) biaxial strains. ε_h, ε_u and ε_b are hydrostatic, uniaxial and biaxial strains applied to the tungsten lattice, respectively.

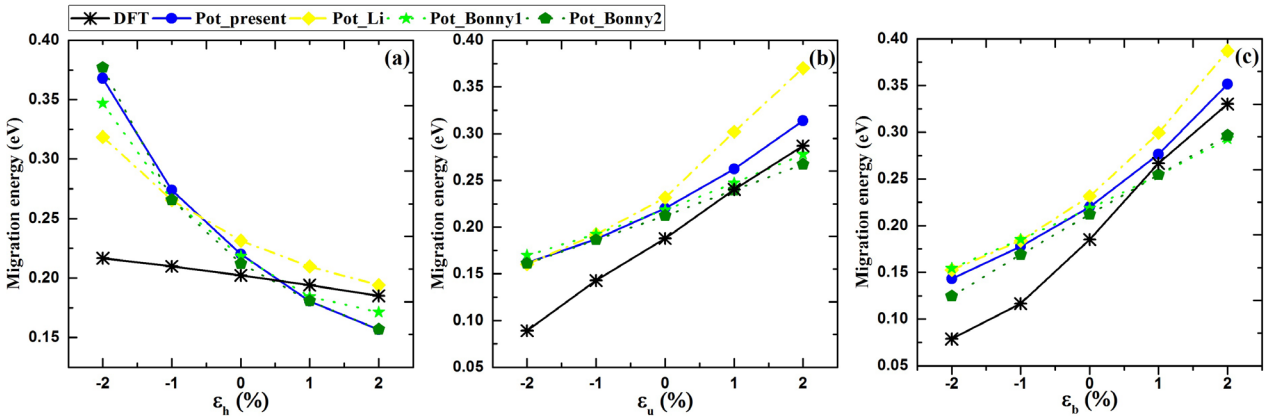

Figure 10. Migration energy of a hydrogen atom between TISs (from TIS1 to TIS2 in figure 8) in bcc tungsten as a function of (a) hydrostatic, (b) uniaxial, and (c) biaxial strains. ε_h, ε_u and ε_b are hydrostatic, uniaxial and biaxial strains applied to the tungsten lattice, respectively.

hydrogen binding energy predicted by Pot_Bonny1 has an obvious breakpoint at $n/m = 1$, indicating there are two different binding models describing the interaction between hydrogen and vacancy clusters depending on which constituent is more in the cluster. Such result may be caused by the wrong occupation prediction of hydrogen atoms in a monovacancy and the failure in describing hydrogen molecules in vacuum, according to Pot_Bonny1 [19]. Different from Pot_Bonny1, Pot_Bonny2 shows a very scattered sequential hydrogen binding energy, especially when $m > 3$. This indicates that the ground states of a vacancy-hydrogen cluster are much harder to be found by Pot_Bonny2.

3.3. Strain effects on hydrogen solution and diffusion in tungsten

Strains are widely believed to be an important factor in changing the solubility and diffusivity of hydrogen in tungsten. According to Zhou *et al* [61], the solution energy of hydrogen shows a linear dependence on the hydrostatic strain, yet mainly a decrease with the presence of anisotropic strains. The diffusion energy of hydrogen atoms between two neighbor TISs is also explored and found that it decreases (increases) when the hydrostatic tensile (compressive) stress increases [62, 63]. Due to the limitation of interatomic potentials, however, such results have not been fully investigated and reproduced by MD, which makes those simulations involving hydrogen dissolving and diffusing in strained regions, such as surfaces, dislocations or grain-boundaries, are less convincing. Here, therefore, both solution energy of a hydrogen atom in TIS (TIS1 in figure 8) and hydrogen diffusion energy barrier for the hop between TISs (from TIS1 to TIS2 in figure 8) under moderate hydrostatic, uniaxial and biaxial strains are calculated using Pot_present as well as other potentials, and the results are displayed in figures 9 and 10. In particular, the uniaxial strains are loaded along the [1 0 0] direction, and the biaxial strains are loaded along the [1 0 0] and [0 1 0] directions, as shown in figure 8. To verify the performance of the potentials, DFT calculations are carried out, the results of which are also displayed in figures 9 and 10.

As seen from figure 9, under both isotropic and anisotropic strains, the solution energy of hydrogen will decrease with the increase (decrease) of tensile (compressive) strains. Hydrostatic strain shows more significant effects on hydrogen solution than uniaxial and biaxial strains, indicating the solution of hydrogen in tungsten is related to the volume of lattice. The strain-depended solution energy predicted by Pot_present has a satisfying agreement with the DFT calculations, even though it exhibits slight nonlinearity. Other interatomic potentials also predict a linear dependence of solution energy on

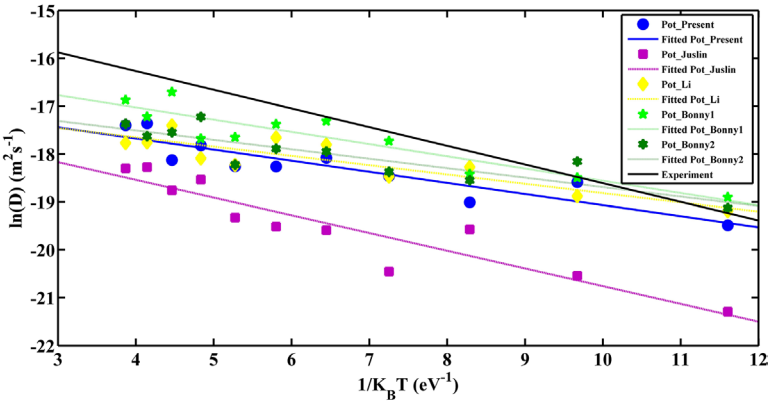

Figure 11. Diffusion data and Arrhenius fits obtained from MD simulations in comparison with Arrhenius fit to experimental data [65].

Table 5. Arrhenius fits of diffusion data of hydrogen at the temperatures from 1000 to 3000 K in tungsten.

Diffusivity	Experiment[a]	Pot_present	Pot_Juslin	Pot_Li	Pot_Bonny1	Pot_Bonny2
Pre-exponential factor (m^2 s^{-1})	4.1×10^{-7}	5.3×10^{-8}	3.9×10^{-8}	4.7×10^{-8}	1.1×10^{-7}	5.5×10^{-8}
Activation energy (eV)	0.39	0.23	0.37	0.19	0.26	0.20

[a] Reference [57].

strain. However, both Pot_Juslin and Pot_Li display a steeper energy-strain line than the DFT calculations, indicating that the solution energy of hydrogen derived from Pot_Juslin and Pot_Li may be more sensitive to strains. Pot_Bonny1 and Pot_Bonny2 display a much higher and lower solution energy, respectively, even though they both qualitatively agree with the DFT calculations. Overall, Pot_present predicts more accurate solution energy of hydrogen with the presence of strains in tungsten and shows good transferability.

The migration energy of a hydrogen atom between two TISs responses differently to isotropic and anisotropic strains, as shown in figure 10. Under hydrostatic strain, the migration energy decreases as the compressive (tensile) strain decreases (increases), while under uniaxial and biaxial strains, the migration energy increases as the compressive (tensile) strain decreases (increases). Both Pot_present and other interatomic potentials exhibit an acceptable agreement with the DFT calculations, as shown in figure 10. In particular, even though the migration energy predicted by the potentials responses to hydrostatic strains more sensitively than that predicted by the DFT calculations, there is a basic qualitative match between them. As for uniaxial and biaxial strains, the results obtained from the potentials agree with DFT calculations both qualitatively and quantitatively.

3.4. Hydrogen diffusion in tungsten

The diffusional properties of hydrogen in metals are unique since hydrogen is the lightest element and extremely mobile even at low temperatures [64]. In tungsten, the property of hydrogen diffusion will affect hydrogen retention, outgassing and defect formation, all of which are key issues in PFM studies. There have been many investigations focus on the hydrogen diffusivity in tungsten. Frauenfelder *et al* reported the hydrogen diffusivity in tungsten is $D = 4.1 \times 10^{-7}\exp\left(-\frac{0.39\ eV}{k_B T}\right)$ m^2 s^{-1} at temperature from 1200 K to 2400 K based on hydrogen degassing and permeation experiments [65]. Recently, Ikeda *et al* employed the tritium tracer technique for determining hydrogen diffusion coefficients and permeation rate near room temperature for tungsten and proposed diffusion coefficients: $D = (3.8 \pm 0.4) \times 10^{-7}\exp\left(-\frac{(0.40\pm0.02)\ eV}{RT}\right)$ m^2 s^{-1} [66]. Many atomic simulations have also been derived for studying hydrogen diffusivity in tungsten. Calculations based on DFT reported that the height of the migration barrier of hydrogen in tungsten is about 0.21 eV [39, 47, 67]. The hydrogen diffusivity calculated by MD at temperature form 200 K to 3000 K is $D = 5.13 \times 10^{-8}\exp\left(-\frac{0.21\ eV}{k_B T}\right)$ m^2 s^{-1} [68]. KMC simulations are also performed to quantify the hydrogen diffusivity in tungsten, which report $D = 1.58 \times 10^{-7}\exp\left(-\frac{0.25\ eV}{k_B T}\right)$ m^2 s^{-1} [69] and $D = 8.45 \times 10^{-7}\exp\left(-\frac{0.440\ eV}{k_B T}\right)$ m^2 s^{-1} [70], respectively. It seems that almost all the atomic simulations underestimate the diffusivity of hydrogen, especially the migration energy, compared with experimental results. However, recently Ahlgren *et al* proposed a new analysis method to determine diffusion coefficients and indicated that the hydrogen migration barrier should be 0.25 eV instead of 0.39 eV, which is consistent with the simulation results [71].

In consideration of the significance of hydrogen diffusivity in tungsten, here, we carry out MD simulation to investigate the hydrogen diffusion properties in tungsten using Pot_present, which could also be a verification for Pot_present on performing thermodynamic simulation. The mean square displacements of a hydrogen atom in tungsten is calculated at a wide temperature range of 1000 K to 3000 K, and the data points are fitted by the Arrhenius law:

$$D = D_0\exp\left(\frac{-E_A}{k_B T}\right) \tag{21}$$

Table 6. A summarization on the potential assessments. Symbol '√' represents that the potential is consistent with DFT calculations or experiments qualitatively, symbol '☆' represents that the potential is consistent with DFT calculations or experiments quantitatively, and the symbol '×' represents that the potential's performance is not reasonable, which neither qualitatively nor quantitatively agrees with DFT calculations and experiments. $E^{H}_{f,ss}$, $E^{H}_{f,tet}$ and $E^{H}_{f,oct}$ are the formation energy of a hydrogen atom at substitutional, tetrahedral interstitial, and octahedral interstitial sites in bcc tungsten, respectively. $E^{H}_{m,t\to t}$ is the migration energy of a hydrogen atom between two nearest neighbor TISs in bcc tungsten.

Properties		Pot_present	Pot_Juslin	Pot_Li	Pot_Bonny1	Pot_Bonny2
Point defect properties of hydrogen	$E^{H}_{f,ss}$	√☆	√☆	√☆	√	√
	$E^{H}_{f,tet}$	√☆	√☆	√☆	√	√
	$E^{H}_{f,oct}$	√☆	√☆	√☆	√	√
	$E^{H}_{m,t\to t}$	√☆	√☆	√☆	√☆	√☆
Hydrogen molecule formation		√☆	√☆	√☆	×	×
Interaction between hydrogen in a perfect tungsten		√☆	×	×	√☆	×
Interaction between hydrogen and a [1 1 1] SIA		√	×	√	√	√
Interaction between hydrogen and a monovacancy		√	×	√	√	√
Interaction between hydrogen and vacancy clusters		√	×	×	×	×
Hydrogen solution in strained tungsten		√☆	√☆	√☆	√	√
Hydrogen diffusion in strained tungsten		√	×	√	√	√
Thermal diffusion of hydrogen in tungsten	Pre-exponential factor	√	√	√	√☆	√
	Activation energy	√	√☆	√	√	√

where D is diffusion coefficient, D_0 is pre-exponential factor, E_A is activity energy, and T is the temperature. For comparison, the diffusivity of hydrogen in tungsten based on other interatomic potentials is also derived, and data from experiment [65] is referred. All the simulation results and fittings are plotted and listed in figure 11 and table 5. Obviously, all the interatomic potentials including Pot_present underestimate the diffusivity of hydrogen in tungsten compared with experimental data, particularly at high temperatures. However, considering the large uncertainty in the experimental data ($D_0 = 4.1^{+5.0}_{-2.0} \times 10^{-7}$ m s^{-2}, $E_A = 0.39 \pm 0.09$ eV) and the trapping effects of defects which are unavoidable in experiments, the results are in reasonable agreement with experimental data, indicating good performance and transferability of Pot_present.

4. Conclusion

An EAM potential has been developed for modeling hydrogen in tungsten, and an extensive database containing various energetic properties and atomic configurations calculated by DFT is employed to fit the tungsten–hydrogen and hydrogen–hydrogen interaction using a relaxation-fitting approach.

Both the accuracy and transferability of the new potential have been validated by a comprehensive evaluation with respect to the point defect properties of hydrogen, the interaction between hydrogen and various defects in tungsten, the strain effects on the solution and diffusion of hydrogen, and the thermal diffusivity of hydrogen at different temperatures. For comparison, the results based on other tungsten–hydrogen potentials are also derived and assessed. DFT calculations, which are either from the published results or from our own calculations, and available experimental data are both referred as evaluation criterions. A summarization on these assessments is presented to offer a clearer view on the performances of these potentials, as shown in table 6. Pot_present has a very good performance on reproducing the point defect properties of hydrogen, hydrogen molecule formation, interaction between hydrogen atoms in a perfect tungsten, and hydrogen solution in strained tungsten. Results of calculating interaction between hydrogen and SIAs, interplay between hydrogen and vacancies, hydrogen diffusion in strained tungsten, and hydrogen thermal diffusion qualitatively agree with DFT calculations and experiments, even though they are not quantitatively accurate. Compared with other tungsten–hydrogen potentials, Pot_present exhibits an overall better agreement with the DFT calculations and experiments, and shows satisfying transferability.

Interplay between hydrogen and extended defects including [1 1 1] SIAs and vacancy clusters have been investigated on detail using the new potential as well as other potentials. MS calculations show that there is considerable attractive interaction (~0.4 eV) between hydrogen and [1 1 1] SIAs, indicating SIAs could offer trapping sites for hydrogen atoms and hydrogen may lower the mobility of [1 1 1] SIAs. The strong attractive interaction between hydrogen and vacancy clusters is also confirmed by the new potential. It is found the most supported ratio of hydrogen atoms to vacancies in tungsten is about 5, and hydrogen becomes less well bound to clusters as the inventory increases. In addition, we have employed the new potential to investigate hydrogen solution and diffusion in strained tungsten. It is found tensile (compressive) stress facilitates (impedes) hydrogen solution, and isotropic tensile (compressive) stress impedes (facilitates) hydrogen diffusion while anisotropic tensile (compressive) stress facilitates (impedes) hydrogen diffusion.

Based on these results, it is suggested that the new potentials provides a good opportunity to further study hydrogen-defect dynamics and evolutions in tungsten, which may help solve many critical problems that tungsten is facing as a functional material.

Acknowledgments

This work is supported by the National Magnetic Confinement Fusion Program through Grant No. 2013GB109002 and the National Natural Science Foundation of China (NSFC) through Grant No. 51001006. G H Lu acknowledges support from China National Funds for Distinguished Young Scientists through Grant No. 51325103.

ORCID iDs

Fei Gao https://orcid.org/0000-0002-0408-549X

References

[1] `t Hoen M H J, Balden M, Manhard A, Mayer M, Elgeti S, Kleyn A W and van Emmichoven P A Z 2014 Surface morphology and deuterium retention of tungsten after low- and high-flux deuterium plasma exposure *Nucl. Fusion* **54** 083014

[2] Balden M, Lindig S, Manhard A and You J-H 2011 D-2 gas-filled blisters on deuterium-bombarded tungsten *J. Nucl. Mater.* **414** 69–72

[3] Shu W M 2008 High-dome blisters formed by deuterium-induced local superplasticity *Appl. Phys. Lett.* **92** 211904

[4] Alimov V K and Roth J 2007 Hydrogen isotope retention in plasma-facing materials: review of recent experimental results *Phys. Scr.* **2007** 6

[5] Tokunaga K, Baldwin M J, Doerner R P, Noda N, Kubota Y, Yoshida N, Sogabe T, Kato T and Schedler B 2005 Blister formation and deuterium retention on tungsten exposed to low energy and high flux deuterium plasma *J. Nucl. Mater.* **337** 887–91

[6] Denkevits A and Dorofeev S 2005 Dust explosion hazard in ITER : explosion indices of fine graphite and tungsten dusts and their mixtures *Fusion Eng. Des.* **79** 1135–9

[7] Bacharis M, Coppins M, Fundamenski W and Allen J E 2012 Modelling of tungsten and beryllium dust in ITER *Plasma Phys. Control. Fusion* **54** 85010

[8] Hatano Y *et al* 2013 Trapping of hydrogen isotopes in radiation defects formed in tungsten by neutron and ion irradiations *J. Nucl. Mater.* **438** S114–9

[9] Tanabe T 2014 Review of hydrogen retention in tungsten *Phys. Scr.* **T159** 14044

[10] Shimada M, Cao G, Hatano Y, Oda T, Oya Y, Hara M and Calderoni P 2011 The deuterium depth profile in neutron-irradiated tungsten exposed to plasma *Phys. Scr.* **T145** 14051

[11] Hatano Y, Shimada M, Oya Y, Cao G, Kobayashi M, Hara M, Merrill B J, Okuno K, Sokolov M A and Katoh Y 2013 Retention of hydrogen isotopes in neutron irradiated tungsten *Mater. Trans.* **54** 437–41

[12] Wright G M, Mayer M, Ertl K, de Saint-Aubin G and Rapp J 2010 Hydrogenic retention in irradiated tungsten exposed to high-flux plasma *Nucl. Fusion* **50** 75006

[13] Philipps V 2011 Tungsten as material for plasma-facing components in fusion devices *J. Nucl. Mater.* **415** S2–9

[14] Gao L, Jacob W, von Toussaint U, Manhard A, Balden M, Schmid K and Schwarz-Selinger T 2017 Deuterium supersaturation in low-energy plasma-loaded tungsten surfaces *Nucl. Fusion* **57** 16026

[15] Barton J L, Wang Y Q, Doerner R P and Tynan G R 2016 Model development of plasma implanted hydrogenic diffusion and trapping in ion beam damaged tungsten *Nucl. Fusion* **56** 106030

[16] McCreery J H and Wolken G 1975 A model potential for chemisorption: {H}_2 + {W}(0 0 1) *J. Chem. Phys.* **63** 2340–9

[17] Juslin N, Erhart P, Träskelin P, Nord J, Henriksson K O E, Nordlund K, Salonen E and Albe K 2005 Analytical interatomic potential for modeling nonequilibrium processes in the W–C–H system *J. Appl. Phys.* **98** 123520

[18] Li X C, Shu X, Liu Y N, Gao F and Lu G H 2011 Modified analytical interatomic potential for a W–H system with defects *J. Nucl. Mater.* **408** 12–7

[19] Bonny G, Grigorev P and Terentyev D 2014 On the binding of nanometric hydrogen–helium clusters in tungsten *J. Phys.: Condens. Matter* **26** 485001

[20] Marinica M-C, Ventelon L, Gilbert M R, Proville L, Dudarev S L, Marian J, Bencteux G and Willaime F 2013 Interatomic potentials for modelling radiation defects and dislocations in tungsten *J. Phys.: Condens. Matter* **25** 395502

[21] Baskes M I, Sha X, Angelo J E and Moody N R 1997 Trapping of hydrogen to lattice defects in nickel *Model. Simul. Mater. Sci. Eng.* **5** 651–2

[22] Angelo J E, Moody N R and Baskes M I 1995 Trapping of hydrogen to lattice defects in nickel *Model. Simul. Mater. Sci. Eng.* **3** 289–307

[23] Rose J H, Smith J R, Guinea F and Ferrante J 1984 Universal features of the equation of state of metals *Phys. Rev.* B **29** 2963–9

[24] Gao F, Deng H, Heinisch H L and Kurtz R J 2011 A new Fe–He interatomic potential based on *ab initio* calculations in α-Fe *J. Nucl. Mater.* **418** 115–20

[25] Plimpton S 1995 Fast parallel algorithms for short-range molecular dynamics *J. Comput. Phys.* **117** 1–19

[26] Henkelman G and Jónsson H 2000 Improved tangent estimate in the nudged elastic band method for finding minimum energy paths and saddle points *J. Chem. Phys.* **113** 9978–85

[27] Henkelman G, Uberuaga B P and Jónsson H 2000 Climbing image nudged elastic band method for finding saddle points and minimum energy paths *J. Chem. Phys.* **113** 9901–4

[28] Hoover W G 1985 Canonical dynamics: equilibrium phase-space distributions *Phys. Rev.* A **31** 1695–7

[29] Shinoda W, Shiga M, Mikami M and Carlo M 2004 Rapid estimation of elastic constants by molecular dynamics simulation under constant stress *Phys. Rev.* B **69** 134103

[30] Martyna G J, Tobias D J and Klein M L 1994 Constant pressure molecular dynamics algorithms *J. Chem. Phys.* **101** 4177

[31] Parrinello M and Rahman A 1981 Polymorphic transitions in single crystals: a new molecular dynamics method *J. Appl. Phys.* **52** 7182–90

[32] Tuckerman M E, Alejandre J, López-Rendón R, Jochim A L and Martyna G J 2006 A Liouville-operator derived measure-preserving integrator for molecular dynamics simulations in the isothermal–isobaric ensemble *J. Phys. A: Math. Gen.* **39** 5629

[33] Kresse G and Hafner J 1993 *Ab initio* molecular dynamics for liquid metals *Phys. Rev.* B **47** 558–61

[34] Kresse G and Furthmüller J 1996 Efficient iterative schemes for *ab initio* total-energy calculations using a plane-wave basis set *Phys. Rev.* B **54** 11169–86

[35] Perdew J P and Wang Y 1992 Accurate and simple analytic representation of the electron–gas correlation energy *Phys. Rev.* B **45** 13244–9

[36] Blöchl P E 1994 Projector augmented-wave method *Phys. Rev.* B **50** 17953–79

[37] Pack J D and Monkhorst H J 1977 'Special points for Brillouin-zone integrations'-a reply *Phys. Rev.* B **16** 1748–9

[38] Lu G H, Zhou H B and Becquart C S 2014 A review of modelling and simulation of hydrogen behaviour in tungsten at different scales *Nucl. Fusion* **54** 86001

[39] Liu Y L, Zhang Y, Luo G N and Lu G H 2009 Structure, stability and diffusion of hydrogen in tungsten: a first-principles study *J. Nucl. Mater.* **390–1** 1032–4
[40] Henriksson K O E, Nordlund K, Krasheninnikov A and Keinonen J 2005 Difference in formation of hydrogen and helium clusters in tungsten *Appl. Phys. Lett.* **87** 1–3
[41] Xu J and Zhao J 2009 First-principles study of hydrogen in perfect tungsten crystal *Nucl. Instrum. Methods Phys. Res.* B **267** 3170–4
[42] Becquart C S and Domain C 2009 A density functional theory assessment of the clustering behaviour of He and H in tungsten *J. Nucl. Mater.* **386–8** 109–11
[43] Heinola K, Ahlgren T, Nordlund K and Keinonen J 2010 Hydrogen interaction with point defects in tungsten *Phys. Rev.* B **82** 1–5
[44] Kato D, Iwakiri H, Watanabe Y, Morishita K and Muroga T 2015 Super-saturated hydrogen effects on radiation damages in tungsten under the high-flux divertor plasma irradiation *Nucl. Fusion* **55** 83019
[45] Fernandez N, Ferro Y and Kato D 2015 Hydrogen diffusion and vacancies formation in tungsten: density functional theory calculations and statistical models *Acta Mater.* **94** 307–18
[46] Sun L, Jin S, Li X C, Zhang Y and Lu G H 2013 Hydrogen behaviors in molybdenum and tungsten and a generic vacancy trapping mechanism for H bubble formation *J. Nucl. Mater.* **434** 395–401
[47] Johnson D F and Carter E A 2010 Hydrogen in tungsten: absorption, diffusion, vacancy trapping, and decohesion *J. Mater. Res.* **25** 315–27
[48] Liu Y L, Zhang Y, Zhou H B, Lu G H, Liu F and Luo G N 2009 Vacancy trapping mechanism for hydrogen bubble formation in metal *Phys. Rev.* B **79** 172103
[49] Bukonte L, Ahlgren T and Heinola K 2014 Modelling of monovacancy diffusion in W over wide temperature range *J. Appl. Phys.* **115** 123504
[50] Liu Y L, Zhou H B and Zhang Y 2011 Investigating behaviors of H in a W single crystal by first-principles: from solubility to interaction with vacancy *J. Alloys Compd.* **509** 8277–82
[51] Middleburgh S C, Voskoboinikov R E, Guenette M C and Riley D P 2014 Hydrogen induced vacancy formation in tungsten *J. Nucl. Mater.* **448** 270–5
[52] Kato D, Iwakiri H and Morishita K 2011 Formation of vacancy clusters in tungsten crystals under hydrogen-rich condition *J. Nucl. Mater.* **417** 1115–8
[53] Kato D, Iwakiri H and Morishita K 2009 First-principle study on binding energy of vacancy-hydrogen cluster in tungsten *J. Plasma Fusion Res. Ser.* **8** 404–7
[54] Ohsawa K, Goto J, Yamakami M, Yamaguchi M and Yagi M 2010 Trapping of multiple hydrogen atoms in a tungsten monovacancy from first principles *Phys. Rev.* B **82** 1–6
[55] Ventelon L, Willaime F, Fu C C, Heran M and Ginoux I 2012 *Ab initio* investigation of radiation defects in tungsten: structure of self-interstitials and specificity of di-vacancies compared to other bcc transition metals *J. Nucl. Mater.* **425** 16–21
[56] You Y W, Kong X S, Wu X B, Xu Y C, Fang Q F, Chen J L, Luo G N, Liu C S, Pan B C and Wang Z 2013 Dissolving, trapping and detrapping mechanisms of hydrogen in bcc and fcc transition metals *AIP Adv.* **3** 012118
[57] Liu Y-N, Ahlgren T, Bukonte L, Nordlund K, Shu X, Yu Y, Li X-C and Lu G-H 2013 Mechanism of vacancy formation induced by hydrogen in tungsten *AIP Adv.* **3** 122111
[58] Miyamoto M, Nishijima D, Ueda Y, Doerner R P, Kurishita H, Baldwin M J, Morito S, Ono K and Hanna J 2009 Observations of suppressed retention and blistering for tungsten exposed to deuterium–helium mixture plasmas *Nucl. Fusion* **49** 65035
[59] Zayachuk Y, Tanyeli I, Van Boxel S, Bystrov K, Morgan T W and Roberts S G 2016 Combined effects of crystallography, heat treatment and surface polishing on blistering in tungsten exposed to high-flux deuterium plasma *Nucl. Fusion* **56** 86007
[60] Shu W M, Wakai E and Yamanishi T 2007 Blister bursting and deuterium bursting release from tungsten exposed to high fluences of high flux and low energy deuterium plasma *Nucl. Fusion* **47** 201–9
[61] Zhou H B, Jin S, Zhang Y, Lu G H and Liu F 2012 Anisotropic strain enhanced hydrogen solubility in bcc metals: the independence on the sign of strain *Phys. Rev. Lett.* **109** 135502
[62] Dong N, Zhang C, Liu H, Li J, Wu X and Han P 2014 Stress effects on stability and diffusion behavior of sulfur impurity in nickel: a first-principles study *Comput. Mater. Sci.* **90** 137–42
[63] Ding W, He H, Liu C, Ding R, Chen J and Pan B 2014 Strain-dependent diffusion behavior of H within tungsten *Physica* B **443** 76–9
[64] Hempelmann R 1984 Diffusion of hydrogen in metals *J. Less Common Met.* **101** 69–96
[65] Frauenfelder R 1969 Solution and diffusion of hydrogen in tungsten *J. Vac. Sci. Technol.* **6** 388
[66] Ikeda T, Otsuka T and Tanabe T 2011 Application of tritium tracer technique to determination of hydrogen diffusion coefficients and permeation rate near room temperature for tungsten *Fusion Sci. Technol.* **60** 1463–6
[67] Heinola K and Ahlgren T 2016 Diffusion of hydrogen in bcc tungsten studied with first principle calculations diffusion of hydrogen in bcc tungsten studied with first principle *J. Appl. Phys.* **107** 113531
[68] Liu Y-N, Wu T, Yu Y, Li X-C, Shu X and Lu G-H 2014 Hydrogen diffusion in tungsten: a molecular dynamics study *J. Nucl. Mater.* **455** 676–80
[69] Oda T, Zhu D and Watanabe Y 2015 Kinetic Monte Carlo simulation on influence of vacancy on hydrogen diffusivity in tungsten *J. Nucl. Mater.* **467** 439–47
[70] Yang X and Hassanein A 2014 Kinetic Monte Carlo simulation of hydrogen diffusion on tungsten reconstructed (0 0 1) surface *Fusion Eng. Des.* **89** 2545–9
[71] Ahlgren T and Bukonte L 2016 Concentration dependent hydrogen diffusion in tungsten *J. Nucl. Mater.* **479** 195–201
[72] Lee S C, Choi J H and Lee J G 2009 *J. Nucl. Mater.* **383** 244